Enhanced Seeing Mode at the LBT: A Method to Significantly Improve Angular Resolution over a 4′ × 4′ Field of View

Barry Rothberg[a,b], Julian C. Christou[a], Douglas L. Miller[a], Dave Thompson[a], Gregory E. Taylor[a], and Christian Veillet[a]

[a]Large Binocular Telescope Observatory, 933 North Cherry Avenue, Tucson, AZ 85721, USA
[b]Department of Physics and Astronomy, George Mason University, MS 3F3, 4400 University Drive, Fairfax, VA 22030, USA

ABSTRACT

Since 2014, the LBT's First Light Adaptive Optics (FLAO) system has also included a seldom used capability, known as Enhanced Seeing Mode (ESM), that can improve the angular resolution over a 4′ × 4′ field of view (FOV). In full AO operation, FLAO provides diffraction limited (DL) capabilities over a small ($30'' \times 30''$) FOV. By comparison, ESM can achieve significantly enhanced resolution, over natural seeing, across a far larger FOV. This improves operational efficiency over standard seeing limited (SL) observations and is applicable across a broader range of scientific targets. ESM uses 11 modes of correction (including tip and tilt) to remove residual aberrations and jitter which significantly improves angular resolution over the full FOV. While this mode does not reach the DL, it can achieve uniform angular resolutions as good as $0''.22$ over the FOV. Furthermore, it allows for the use of multi-object spectroscopy with R∼10,000 or imaging with angular resolution similar to that achieved by the Wide-Field Camera 3 infrared channel on the Hubble Space Telescope, but powered by 11.6 meters of effective aperture in binocular mode. As part of the on-going characterization of ESM, we have demonstrated that even in poor seeing conditions ($\theta \sim 1''.5$-$2''$) the image quality delivered to the focal station is improved by factors of 2-3. Here, we present the first results of the characterization of ESM, including systematic tests of the delivered PSF across the FOV as a function of the brightness of, and distance from, the AO Reference Star. We present a range of galactic and extra-galactic targets showing the improvements obtained over a broad range of seeing conditions and propose ESM as a standard observational mode for near-Infrared observations.

Keywords: Adaptive Optics, ELT, Observatories, Instrumentation, Binocular

1. INTRODUCTION

1.1 The Large Binocular Telescope

The Large Binocular Telescope (LBT) is located on Emerald Peak (elevation 3,192 meters) on Mount Graham, which is located in southeastern Arizona near the city of Safford. The observatory operates from September 1-July 10 each year. Between July 11 and August 31 the observatory closes for monsoon season and this down-time is used for telescope and instrument maintenance and upgrades. The LBT is an international partnership which includes: the University of Arizona, Arizona State University and Northern Arizona University (25% share of time); Germany or LBT Beteiligungsgesellschaft (25% share of time), which includes the German institutes of Landessternwarte Königstuhl, Leibniz Institute for Astrophysics Potsdam (AIP), Max-Planck-Institut für Astronomie, Max-Planck-Institut für Extraterrestrische Physik, and Max-Planck-Institut für Radioastronomie. Some of this time is also allocated to public universities within Germany; Italy or Instituto Nazionale di Astrofisica (25% share of time), which offers access to the entire Italian astronomical community; The Ohio State University (12.5% share of time); and the Research Corporation for Science and Advancement (12.5% share of time) which coordinates the participation of four universities (The Ohio State University, University of Notre Dame,

Further author information: (Send correspondence to Barry Rothberg)
E-mail: brothberg@lbto.org, Telephone: +1 520 626-8672, Fax: +1 520 626-9333

University of Minnesota, and University of Virginia).

The Large Binocular Telescope houses two 8.4 meter primary mirrors, separated by 14.4 meters (center-to-center), affixed to a single compact altitude-azimuth mount housed in a co-rotating enclosure, see Hill et al. (2004),[1] Hill et al. (2010)[2] and references therein for more details. Each mirror has four Bent Gregorian focal stations, a direct Gregorian focal station, and a swing arm which houses a prime focus optical camera. Another swing arm houses the adaptive secondary mirror which is placed into the beam when the prime focus camera is not being used. A third swing arm moves and aligns tertiary mirror with the requested Bent Gregorian focal station. The transition between prime focus and Gregorian instruments takes $\sim$ 20 minutes, while transitions between different Gregorian instruments can take $\leq$ 10 minutes. The left-side of the telescope is denoted as SX (the 'S' from the Italian word for left, *sinistra*), and the right-side is denoted as DX (the 'D' from the Italian word for right, *destra*).

The unique design of LBT allows for its use in three configurations: 1) "Twinned" or Duplex mode in which each mirror has identical instrument configurations yielding an effective collecting area of $\simeq$ 11.6 meters; 2) Interferometric mode which uses the baseline between mirrors to create an effective aperture of 22.6 meters; and 3) "Heterogeneous" mode, in which the 8.4 meter primary mirrors are each configured with different instruments or different modes of the same instruments (i.e. optical on SX, near-IR on DX, or optical imaging on SX and optical spectroscopy on DX) and operate as two independent telescopes on a common mount. In this mode, the two mirrors can move independently of each other up to the "co-pointing limit" ($\sim 40''$), (e.g. Rakich et al. 2011,[3] Hill et al. 2014,[4] Rothberg et al. 2018[5]).

1.2 First Light Adaptive Optics (FLAO) System

The Natural Guide Star (NGS) adaptive optics system at LBT uses an Adaptive Secondary Mirror with 672 actuators driving a deformable shell. A pyramid wavefront sensor uses the brightness and point-spread function (PSF) of an NGS to apply corrections for atmospheric turbulence. Currently, the First Light Adaptive Optics (FLAO) system offers from 36 to 400 modes of corrections for full diffraction limited (DL) AO. It can correct for non-common path aberrations (NCPA) using on-axis bright natural guide-stars (Esposito et al. 2010,[6] 2012,[7] Christou et al. 2016,[8] 2018,[9] and Miller et al. 2016.[10] The corrections need to achieve a DL PSF are directly related to the brightness of the NGS, the angular separation between it and the science target, and the wavelength of the observations.

However, FLAO can also apply 11 modes to improve angular resolution: tip, tilt, focus, 2 $\times$ astigmatism, 2 $\times$ coma, 2 $\times$ trefoil, spherical and 1 "high" order. These 11 modes define Enhanced Seeing Mode (ESM). The AO patrol field used for both diffraction limited AO and ESM is $3' \times 2'$ and requires a reference star $m_{\mathrm{R}} \leq$ 16. Currently, the FLAO system is undergoing an upgrade to the next generation Single conjugated adaptive Optics Upgrade for LBT (SOUL). This upgrade will increase the number of modes which can be applied to full DL AO and allow for use of AO Reference Stars 1.5-2 magnitudes fainter than the current limit (Pinna et al. 2016,[11] Christou et al. 2018[9]). The SOUL upgrade is undergoing commissioning on SX and the hardware will be installed on DX during the Fall and Winter of 2019.

1.3 LBT Utility Camera in the Infrared (LUCI)

The two LBT Utility Camera in the Infrared instruments (LUCIs), are a pair of cryogenic near-Infrared (NIR) instruments sensitive from 0.95*-2.4μm with imaging and spectroscopic (longslit and multi object slit) capabilities. Each LUCI houses a 2K $\times$ 2K Hawaii 2RG detector and three cameras which deliver a $0''.25$/pixel (f/1.8 designated N1.8), $0''.12$/ pixel (f/3.75 designated N3.75), or a $0''.015$/pixel (f/30 designated N30) plate scale. The N1.8 camera is only used for seeing limited (SL) spectroscopy. The N30 camera is designed for DL AO and delivers a $30'' \times 30''$ FOV (currently only available in imaging mode). The N3.75 camera yields a $4' \times 4'$ FOV and is used for both SL and ESM imaging and spectroscopy (DL AO is under-sampled with this camera). Each LUCI is mounted at the front bent Gregorian port of SX or DX. Both LUCIs house the same complement of broad-, medium-, and narrow-band filters, but do not have the same spectroscopic gratings. Currently, DL AO spectroscopy is not available (and would only be available on LUCI-2). ESM offers an opportunity to improve both the angular and spectral resolution of longslit and multi-object slit (MOS) spectroscopy by improving the

---

*The dichroic dewar entrance window cut-on is $\sim 0.89\mu$m for LUCI-1 on SX and $\sim 0.95\mu$m for LUCI-2 on DX

signal-to-noise (S/N) and allowing the use of smaller slitwidths. For more information regarding the available filters, gratings, etc, see Rothberg et al. 2018[5] and references therein.

2. CHARACTERIZATION OF ESM

2.1 Early Testing

Using only low order modes to improve angular resolution was a capability already part of the FLAO system from it's inception (Esposito et al. 2011[12] and Esposito et al. 2012[7]). This mode of operation is benefited by the large angular size of the AO Reference Star patrol field, which covers a sizable fraction (more than $1/3^{rd}$) of the full LUCI FOV. The first on-sky test of something resembling ESM was reported in Esposito et al. 2011.[12] The FLAO system was operated in bin mode #4 using only 10 modes with an AO reference star of $m_R = 13.2$ but with a neutral density filter to simulate a star of $m_R \sim 17.2$ The observations were conducted using the InfraRed Test Camera (IRTC - Foppiani et al. 2011[13]). The measured H-band full-width at half maximum (FWHM) of the star was $0''.24$, while open-loop (SL) yielded an H-band FWHM = $0''.41$ (see Section 4.2 and Figure 6 of Esposito et al. 2011[12]).

Figure 1. False color image of the reflection nebula NGC 1931 created from Brackett γ (blue - 160 seconds), K_s (green - 192 seconds), and H_2 (red - 120 seconds) filters on LUCI-1 using ESM. The natural seeing at K_s was $\sim 0''.52$ and $\sim 0''.25$ with ESM. Data were obtained on UT 2004-11-19 and processed by D. Thompson.

Subsequently, ESM was formalized to include 11 modes of corrections in conjunction with the N3.75 camera on LUCI-1 (before LUCI-2 was commissioned) in order to provide improved angular resolution across a wider FOV. Any star can be used as an AO Reference star as long as it is $m_R \leq 16$, falls within the AO patrol field, and does not significantly impact the LUCI detector (i.e. saturate or leave strong persistence). The next tests of ESM were performed on-sky using LUCI-1 imaging in the fall of 2014. The targets included several bright stars and the nebula NGC 1931, which contains a number of young stars with a range of magnitudes fairly well distributed over the LUCI FOV. Figure 1 shows a false color composite image comprised of images taken with the Brackett γ, H_2, and K_s filters. Analysis of the K_s-band data showed a factor of two improvement over the natural seeing. Subsequently, ESM imaging was only been attempted a few times during nighttime science operations with LUCI-1.

2.2 Binocular Testing

Starting in May of 2018, LBTO began a more rigorous characterization of the capabilities of ESM using imaging data. This included binocular LUCI-1 and LUCI-2 observations in order to: 1) obtain SL and ESM data to compare the natural seeing with ESM simultaneously; 2) simultaneous ESM observations to determine whether any significant differences exist between LUCI-1 and LUCI-2 which may affect ESM image quality; 3) observe a range of AO Reference Stars to determine the impact of brightness on the applied corrections; 4) observe stellar fields (globular and open clusters) which provide uniform coverage across the LUCI FOV and cover a range of magnitudes; and 5) observe large resolved objects to quantify improvements as a function of brightness of, and distance from, the AO Reference Star. Early results were presented in Rothberg et al. 2018.[5] Since then additional observations were obtained and analyzed. The characterization project was expanded to include J-, H, and K-band data in order to quantify the improvements across the full wavelength range of the LUCIs and to include revisiting the same fields in order to quantify ESM performance under different natural seeing conditions as well as repetition of performance under the same conditions. Presented here are a broader range of multi-wavelength results. These improvements should equally benefit spectroscopic observations as ESM delivers the improved PSF to the focal plane unit of the LUCIs in which either spectroscopic masks (longslit or MOS) sit or no mask if imaging mode is used.

2.2.1 Improvements in Image Quality at K-band

K-band observations of the north-east (NE) periphery of the Milky Way globular cluster M92 were obtained over two non-contiguous nights using both LUCI-1 and LUCI-2 under seeing conditions that ranged from $0''.70$-$2''.06$ as measured by the Differential Image Motion Monitor (DIMM). These values are corrected to zenith at 0.55μm. ESM data were obtained using AO Reference Stars with $m_R = 9.43$ on both nights and $m_R = 15.17$ on the second night. ESM was turned on for one set of data, then the observations were repeated under SL conditions (ESM off). The data were reduced using `IRAF`. The reduction process includes linearization corrections, bad pixel masking, flat-fielding, background subtraction. The `IRAF` tasks `geomap` and `geotran` were used to rectify each exposure by applying sub-pixel shifts, rotation, and accounting for any distortions from the LUCI optics. The `IRAF` task `daofind` was then used to identify stars in the crowded field for each final mosaic image. Non-astronomical objects and stars near the edges of the FOV were removed using an automated `IDL` routine. The `IRAF` task `radprof` was then used to measure a Gaussian FWHM for every star. For each star the radial distance from the AO Reference Star was computed. Figure 2 shows a plot of the FWHM in angular units of arcseconds plotted against the radial distance from the AO Reference Stars for the two epochs. The left panel shows data SL data and ESM data obtained under poor seeing with LUCI-1. The right panel shows a similar comparison, but taken under excellent natural seeing conditions and using two different AO Reference stars. The left panel shows that under poor seeing conditions ESM can "recover" a night and improve the image quality delivered to the LUCI focal plane by almost a factor of three. Data obtained with LUCI-2 show the same improvement. Additional data taken of other fields (the Milky Way open cluster M52, the Milky Way globular cluster Palomar 2 - see section 3), as well as additional data obtained of M92 show this improvement is repeatable. The right panel in Figure 2 demonstrates that under optimal conditions ESM can achieve a resolution of $0''.23$ or better (~ 2 pixels with the LUCI N3.75 camera). The right panel also shows that the corrections achieved with ESM have a slight dependence on the brightness and distance from the AO Reference Star.
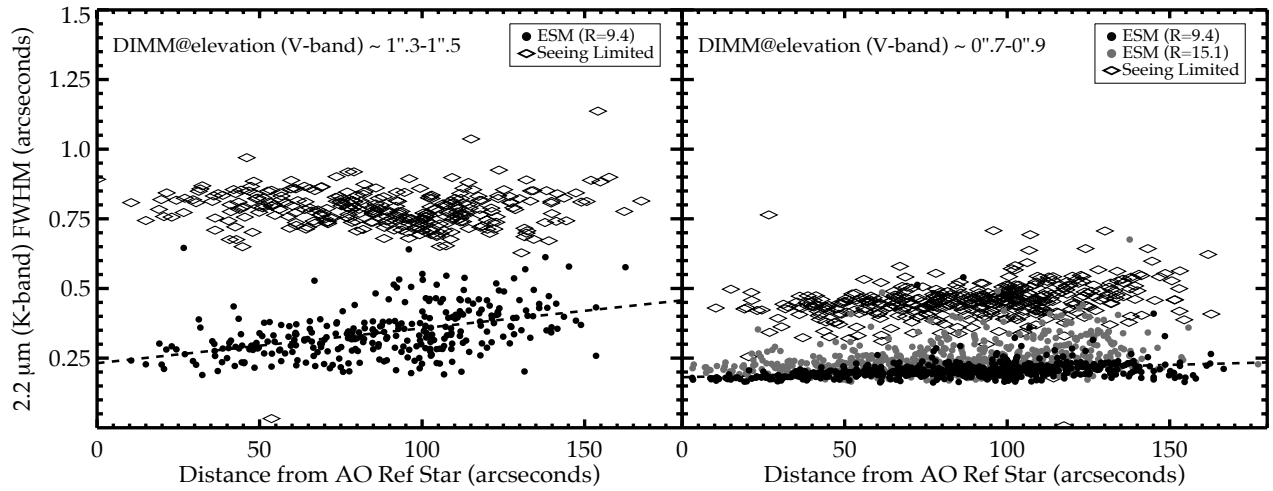
Figure 2. Comparison of SL and ESM values of the FWHM of stars in the NE periphery of the globular cluster M92 as a function of distance from the AO Reference Star (for SL observations this is only to make a direct comparison - the AO Reference Star has no impact on the image quality). The left panel is for data taken under poor natural seeing conditions and shows a 3× improvement of the PSF. The right panel shows the same field taken under excellent natural seeing conditions and adds a second, fainter, AO Reference star for comparison. While the improvement is only a factor of two over SL data, ESM produces a nearly uniform improved PSF of $\theta \sim 0''.23$. The fainter AO Reference star does produce marginally poorer image quality ($\theta \sim 0''.25$). The dotted line is a linear least-squares fit to the data to assess the quality of the improvement. The total integration time for each SL and ESM final mosaic image on the left is 564.75 seconds, and 376.5 seconds on the right.
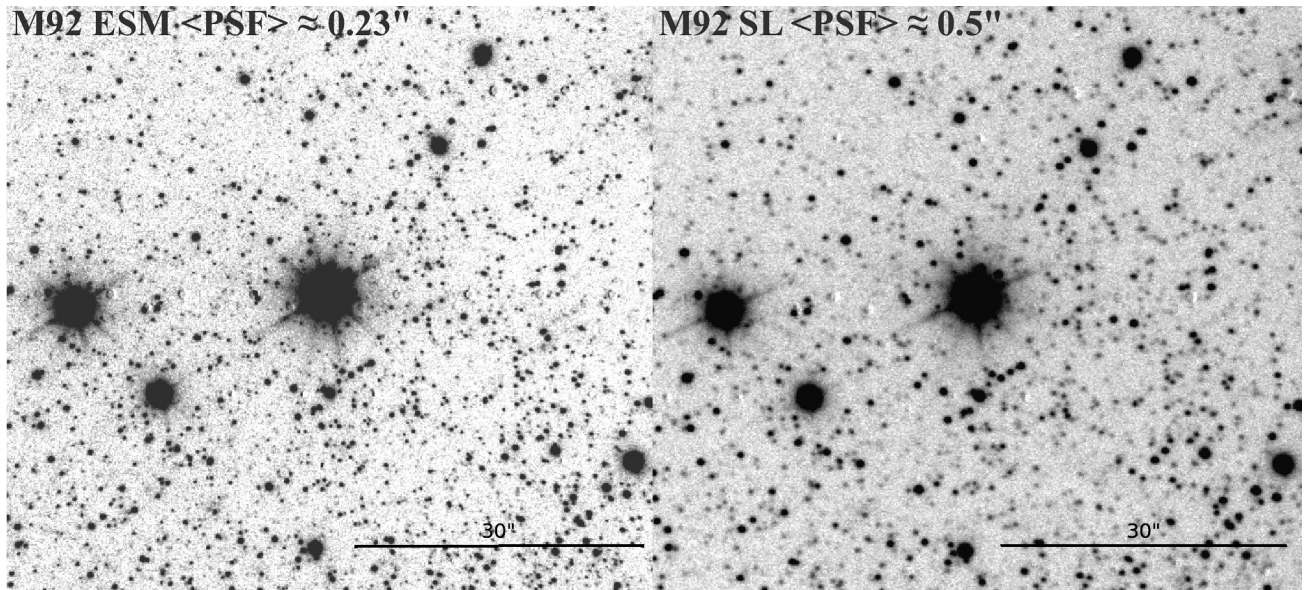

Figure 3. Comparison of the central $1'$ around the $m_{\mathrm{R}} = 9.43$ AO Reference Star for ESM (*left*) and SL (*right*) K-band data of the NE periphery of the Milky Way globular cluster M92. The figure provides a qualitative comparison of the improvement of the PSF and depth achieved in optimal conditions by ESM compared to SL data obtained under excellent natural seeing conditions.

The comparison between SL and ESM observations shown in Figure 3 demonstrates the clear improvement

in sensitivity of ESM over SL observations. The total integration time for each set of K-band observations was 376.5 seconds. Both observations used the same dither pattern, and were processed in the same way using `IRAF`.

2.2.2 J-band Image Quality

As part of the characterization of ESM using large resolved objects and observations at $\lambda < 2\mu$m observations of the advanced (single nucleus) merger remnant NGC 3921 were obtained under poor seeing conditions. NGC 3921 was selected from a larger sample of 51 advanced merger remnants (Rothberg & Joseph 2004[14]). The angular sizes of these objects are all at least 1′ in diameter and have published or archival multi-wavelength ground- and space-based imaging datasets available (i.e. Rothberg & Fischer 2010[15]) allowing for comparisons with ESM performance. NGC 3921 was selected based on visibility and a nearby AO Reference star.
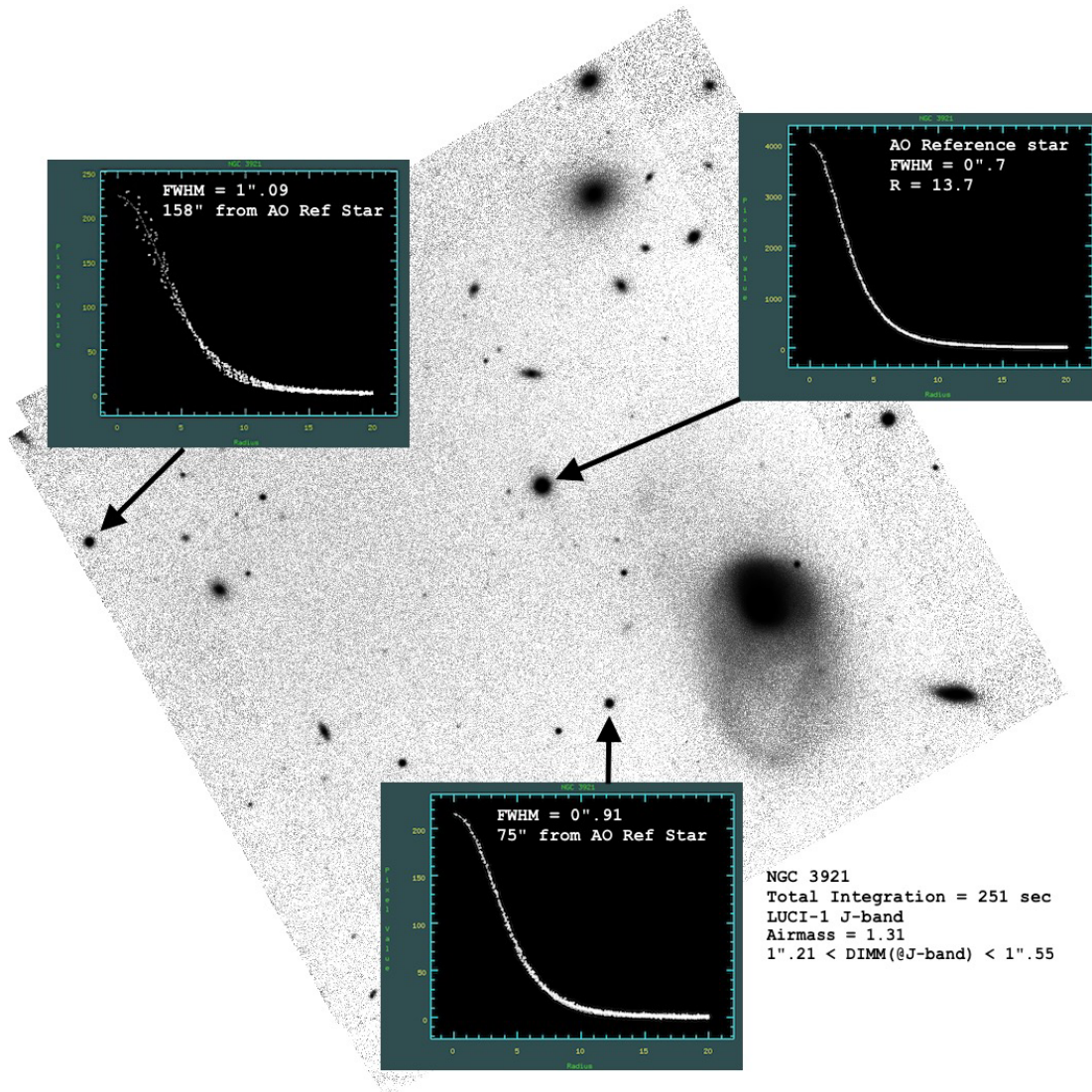

Figure 4. J-band (1.25μm) final mosaic image of the advanced merger remnant NGC 3921 obtained with LUCI-1 using ESM with a $m_\mathrm{R} = 13.7$ AO Reference star. Shown inset are 1D light profiles of various stars in the field, including the AO Reference Star. The DIMM seeing, corrected to J-band and the elevation of the target is shown in the figure. In poor seeing ESM can deliver a factor 70-200% improvement to the LUCI focal plane at J-band.

Preliminary results clearly demonstrate that the image quality at *J*-band can significantly benefit from the use of ESM, even in poor conditions. Figure 4 shows a mosaiced field of NGC 3921 created from four exposures of 62.75 seconds, processed and combined using `IRAF` as described earlier. The data were taken under natural seeing (corrected to *J*-band and the elevation of the target) of $1''.21$-$1''.55$. The 1D light profiles of stars show that the corrections improved the image quality to $\theta = 0''.7$ for the AO Reference Star and to $\theta \sim 0''.9$ near the position of NGC 3921. This type of significant improvement demonstrates the ability to obtain sub-arcsecond quality science data in poor conditions over the full wavelength range of the LUCIs.

3. SCIENTIFIC CASE STUDY FOR ESM - PALOMAR 2

As part of first science demonstration case to test the improvements ESM delivers to the LUCI focal plane, the Milky Way globular cluster Palomar 2 was selected for observations at *J*-, *H*-, and *K*-band. Palomar 2 lies near the anti-center of the Milky Way (relative to Earth) and behind significant patches of interstellar dust. First discovered in 1955 by Abell,[16] it remains one of the least studied GCs. The first distance estimate and stellar census were obtained by Harris (1980).[17] To date, only optical observations of Palomar 2 have been published. LUCI near-IR observations of Palomar 2 were obtained over two non-contiguous nights. ESM observations could only be obtained with LUCI-2 (DX) due to the ongoing commissioning of the SOUL upgrade on SX. SL observations were obtained simultaneously with LUCI-1 on one night allowing for a direct comparison between the natural seeing and the image quality from ESM. Only LUCI-2/ESM observations were obtained on the first night.
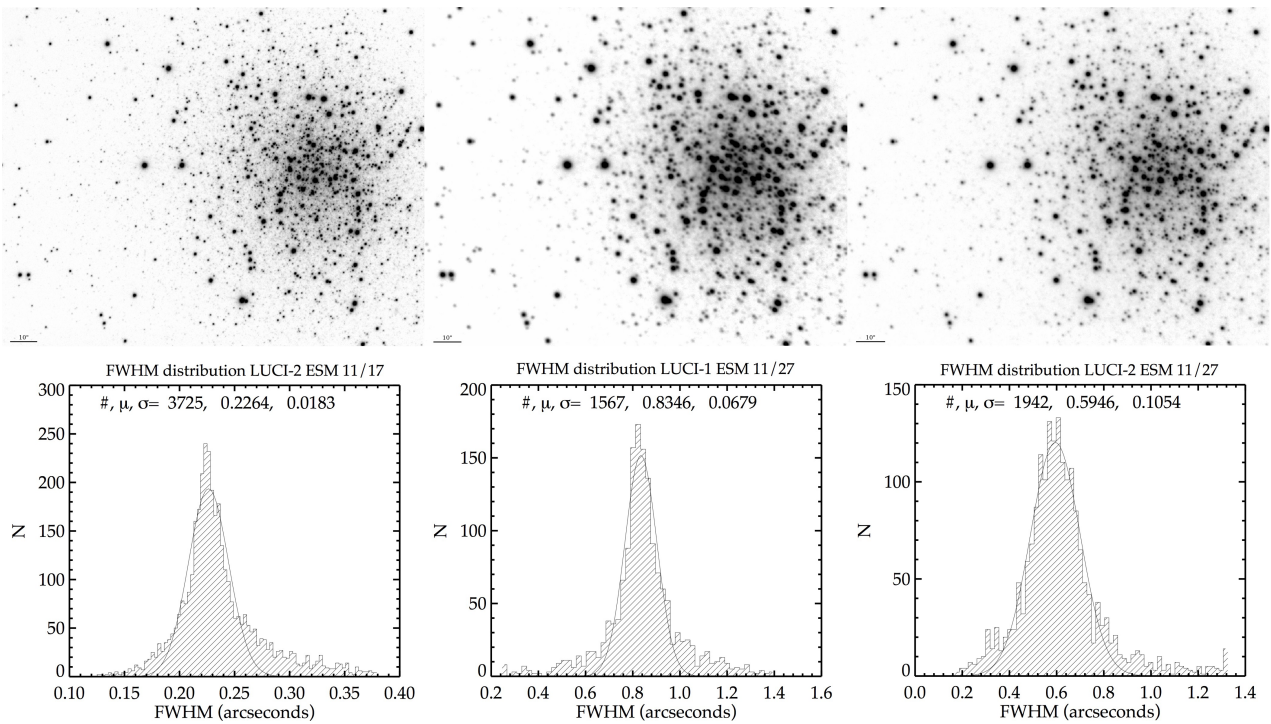

Figure 5. *Top Row*: Comparison of K-band ($2.2\mu m$) images of Palomar 2 obtained with *left* - LUCI-2/ESM - observations with an average *K*-band FWHM $\sim 0''.23$ and an average *V*-band DIMM seeing of $0''.86$ or $0.''65$ (corrected to *K*-band and to the elevation of the observations); *center* - LUCI-1/SL with an average *K*-band FWHM of $0''.83$ and an average *V*-band DIMM seeing of $1''.3$ (corrected to the elevation of the observations); *right* - LUCI-2/ESM observations taken simultaneously with the LUCI-1/SL (*center*). The average *K*-band FWHM of $0''.59$. *Bottom Row*: The distributions of the FWHM measured for all of the objects in each *K*-band image shown above it. Each histogram shows the final number of stars (after sorting to remove spurious detections), the average FWHM in arcseconds (μ), and the 1σ errors in the distribution.

The first part of the analysis measured the image quality of the data. The science frames were processed, aligned, and a final mosaic was created using the `IRAF` procedures described earlier. For the data taken on the 2nd night (UT 2018-11-27), the SL and ESM data were obtained simultaneously allowing for a direct measurement of the real-time improvement of the image quality. This removes any variability or uncertainty from the atmospheric turbulence since the same Cn2 (optical turbulence) profile is applicable to both the SX and DX sides of the telescope. A distribution of the K-band FWHM of the stars in Palomar 2 are shown in Figure 5 for each set of data (bottom row) along with the image of Palomar 2 associated with it (top row). The AO Reference Star used for the observations was listed as $m_R = 12.86$ and was $141''$ away from the core of Palomar 2. However, upon acquisition, it was discovered the "star" was actually a double-star (separated by $1''.5$), but this did not affect closing or maintaining the AO loop each night. The results were consistent with previous observations, in that data obtained under excellent natural seeing conditions yielded a FWHM $\sim 0''.23 \pm 0.01$, even with such a large angular separation between the (double) AO Reference Star and the core of Palomar 2.

Under average seeing conditions during UT 2018-11-27, ESM produced a significant improvement in the PSF. The FWHM improved by $\sim 1.4\times$, from $\theta \sim 0''.83 \pm 0.06$ measured with LUCI-1 to $\theta \sim 0''.59 \pm 0.1$ measured with LUCI-2. Furthermore, the LUCI-2 stellar PSFs were rounder than the SL PSFs of LUCI-1 (see Figure 5).
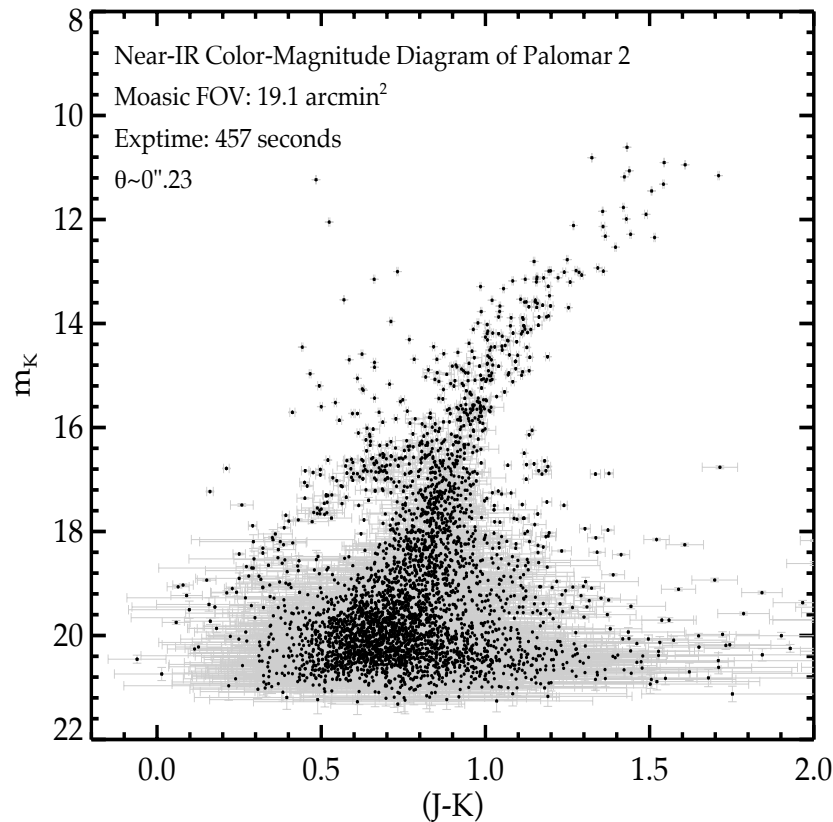

Figure 6. Near-IR Color-Magnitude Diagram (CMD) for Palomar 2 based on data obtained with ESM on UT 2018-11-17. In only 457 seconds, the data are able to achieve a remarkable depth probing to the level of the main sequence turnoff. Each point plotted is shown with error bars.

In addition to assessing the image quality, the data obtained with LUCI-2/ESM on the first of the two nights were used to construct a near-IR color-magnitude diagram (CMD) of Palomar 2. The J-,H-, and K-band images were aligned with each other using the `IRAF` tasks `geomap` and `geotran`. The `IRAF` task `daophot` task was used

to find sources in the crowded field and the task `radprof` was used to measure the FWHM, magnitudes and magnitude errors. The data were first sorted to remove objects with null or INDEF values and magnitude errors ≥ 0.3 mags. The near-IR CMD reaches ~ 1 magnitude deeper in the same integration time (457 seconds in total for each filter) as data obtained from the SL and ESM observations obtained under average conditions. The near-IR CMD is shown in Figure 6 using J-, and K-band data. It clearly shows features such as the main sequence turnoff, asymptotic giant branch stars, and a clump of red giant branch (RGB) stars. The tip of the RGB can be used to infer a distance. Further analysis of this data will be performed and the results presented in a future publication. However, the preliminary results clearly show the power of ESM under excellent seeing conditions in combination with the $4' \times 4'$ LUCI FOV.

4. CONCLUSIONS & FUTURE WORK

The results, to date, indicate that ESM provides a significant improvement in image quality regardless of the natural seeing conditions or the the wavelength (1-2.4μm) observed. While some improvement is expected, the most unexpected result from the analysis so far is the extent of the improvement observed in extremely poor conditions (i.e. $\theta > 1''.5$). The philosophy of the current characterization of ESM is to revisit the same fields multiple times regardless of the atmospheric conditions. This removes systematics (analyzing the same targets in the same way, thus comparing daleks to daleks not daleks to apples) and provides an opportunity to either sample different atmospheric conditions or sample the same atmospheric conditions to verify repeatability of results. In the best natural seeing conditions, the K-band image quality frequently approaches the Nyquist limit of the N3.75 camera. The conclusion thus far is that as long as long as there is a viable AO Reference Star in the patrol field and the FLAO (or in the future, SOUL) system can close and maintain the AO loop, *all* LUCI observations should use, and would benefit from, ESM.

The characterization of ESM is still an ongoing process. Although multi-epoch J-, H-, and K-band data have been collected and reduced for M92 and M52, additional analysis remains to be completed (this includes the corrections achieved with an AO Reference Star at the magnitude limit). In addition to NGC 3921, multi-epoch observations of Hickson Compact Group 31 (HCG 31) have been obtained. Like NGC 3921, the goal is to determine the improvements ESM can provide to resolved objects as a function of the brightness of, and distance from an AO Reference Star. However, HCG 31 contains at least 5 discrete, resolved, galaxies at varying distances from the $m_R = 10.9$ AO Reference Star within the LUCI FOV. These analyses will be presented in a future publication.

With the installation and commissioning of SOUL on SX and the upcoming installation of SOUL on DX, ESM characterization will assess the improvements delivered by these upgrades. Of particular importance is the ability to use fainter AO Reference Stars to provide corrections. SOUL should allow for the use of an AO Reference Star as faint as $m_R \sim 17.5$-18. This opens up a much larger part of the sky for ESM observations and improves the likelihood of finding a suitable AO Reference Star in any given LUCI science field. This will need to be quantified. As shown in Figure 2, there is a weak dependence on the corrections achieved in the image quality as a function of the brightness of the AO Reference Star. Further ESM characterization will be needed to determine the impact of this with the new AO Reference Star limits.

ACKNOWLEDGMENTS

REFERENCES

[1] Hill, J. M. and Salinari, P., "The Large Binocular Telescope project," in [*Ground-based Telescopes*], Oschmann, Jr., J. M., ed., *Proc. SPIE* **5489**, 603–614 (Oct. 2004).

[2] Hill, J. M., Green, R. F., Ashby, D. S., Brynnel, J. G., Cushing, N. J., Little, J., Slagle, J. H., and Wagner, R. M., "The Large Binocular Telescope," in [*Ground-based and Airborne Telescopes III*], *Proc. SPIE* **7733**, 77330C (July 2010).

[3] Rakich, A., Thompson, D., and Kuhn, O. P., "Range-balancing the Large Binocular Telescope," in [*Proc. SPIE*], *Society of Photo-Optical Instrumentation Engineers (SPIE) Conference Series* **8128**, 812808 (Oct 2011).

[4] Hill, J. M., Ashby, D. S., Brynnel, J. G., Christou, J. C., Little, J. K., Summers, D. M., Veillet, C., and Wagner, R. M., "The Large Binocular Telescope: binocular all the time," in [*Ground-based and Airborne Telescopes V*], *Proc. SPIE* **9145**, 914502 (July 2014).

[5] Rothberg, B., Kuhn, O., Power, J., Hill, J. M., Veillet, C., Edwards, M., Thompson, D., and Wagner, R. M., "Current status of the facility instruments at the Large Binocular Telescope Observatory," in [*Ground-based and Airborne Instrumentation for Astronomy VII*], *Proc. SPIE* **10702**, 1070205 (Jul 2018).

[6] Esposito, S., Riccardi, A., Fini, L., Puglisi, A. T., Pinna, E., Xompero, M., Briguglio, R., Quirós-Pacheco, F., Stefanini, P., Guerra, J. C., Busoni, L., Tozzi, A., Pieralli, F., Agapito, G., Brusa-Zappellini, G., Demers, R., Brynnel, J., Arcidiacono, C., and Salinari, P., "First light AO (FLAO) system for LBT: final integration, acceptance test in Europe, and preliminary on-sky commissioning results," in [*Adaptive Optics Systems II*], *Proc. SPIE* **7736**, 773609 (July 2010).

[7] Esposito, S., Riccardi, A., Pinna, E., Puglisi, A. T., Quirós-Pacheco, F., Arcidiacono, C., Xompero, M., Briguglio, R., Busoni, L., Fini, L., Argomedo, J., Gherardi, A., Agapito, G., Brusa, G., Miller, D. L., Guerra Ramon, J. C., Boutsia, K., and Stefanini, P., "Natural guide star adaptive optics systems at LBT: FLAO commissioning and science operations status," in [*Adaptive Optics Systems III*], *Proc. SPIE* **8447**, 84470U (July 2012).

[8] Christou, J. C., Brusa, G., Conrad, A., Esposito, S., Herbst, T., Hinz, P., Hill, J. M., Miller, D. L., Rabien, S., Rahmer, G., Taylor, G. E., Veillet, C., and Zhang, X., "Adaptive optics capabilities at the Large Binocular Telescope Observatory," in [*Adaptive Optics Systems V*], *Proc. SPIE* **9909**, 99092E (July 2016).

[9] Christou, J. C., Brusa, G., Conrad, A., Hill, J., Miller, D. L., Rahmer, G., Taylor, G. E., Veillet, C., and Zhang, X., "Adaptive optics systems at the Large Binocular Telescope: status, upgrades, and improvements," in [*Adaptive Optics Systems VI*], *Proc. SPIE* **10703**, 107030A (Jul 2018).

[10] Miller, D. L., Taylor, G., Christou, J. C., Zhang, X., Brusa Zappellini, G., Rahmer, G., Lefebvre, M., Puglisi, A., Pinna, E., and Esposito, S., "Adaptive optics operations at the Large Binocular Telescope Observatory," in [*Adaptive Optics Systems V*], *Proc. SPIE* **9909**, 99092G (July 2016).

[11] Pinna, E., Esposito, S., Hinz, P., Agapito, G., Bonaglia, M., Puglisi, A., Xompero, M., Riccardi, A., Briguglio, R., Arcidiacono, C., Carbonaro, L., Fini, L., Montoya, M., and Durney, O., "SOUL: the Single conjugated adaptive Optics Upgrade for LBT," in [*Adaptive Optics Systems V*], *Proc. SPIE* **9909**, 99093V (July 2016).

[12] Esposito, S., Riccardi, A., Pinna, E., Puglisi, A., Quirós-Pacheco, F., Arcidiacono, C., Xompero, M., Briguglio, R., Agapito, G., Busoni, L., Fini, L., Argomedo, J., Gherardi, A., Brusa, G., Miller, D., Guerra, J. C., Stefanini, P., and Salinari, P., "Large Binocular Telescope Adaptive Optics System: new achievements and perspectives in adaptive optics," in [*Astronomical Adaptive Optics Systems and Applications IV*], *Proc. SPIE* **8149**, 814902 (Oct 2011).

[13] Foppiani, I., Hill, J. M., Lombini, M., Bregoli, G., Cosentino, G., Diolaiti, E., Herbst, T. M., Innocenti, G., Meschke, D., Miller, D. L., Rohloff, R.-R., and Schreiber, L., "An instrument for commissioning the active and adaptive optics of modern telescopes: the Infrared Test Camera for the Large Binocular Telescope," *Experimental Astronomy* **31**, 115–130 (Oct 2011).

[14] Rothberg, B. and Joseph, R. D., "A Deep K-Band Photometric Survey of Merger Remnants," *AJ* **128**, 2098–2143 (Nov 2004).

[15] Rothberg, B. and Fischer, J., "Unveiling the σ-Discrepancy in Infrared-Luminous Mergers. I. Dust and Dynamics," *ApJ* **712**, 318–349 (Mar 2010).

[16] Abell, G. O., "Globular Clusters and Planetary Nebulae Discovered on the National Geographic Society-Palomar Observatory Sky Survey," *PASP* **67**, 258–261 (Aug 1955).

[17] Harris, W. E., "A note on the characteristics of Palomar 2," *PASP* **92**, 43–45 (Feb 1980).